JOURNAL OF Materials CHEMISTRY

A study of Mn–Ti oxide powders and their behaviour in propane oxidation catalysis

Fabio Milella,*[a] José Manuel Gallardo-Amores,[a,b] Marco Baldi[c] and Guido Busca[a]*

[a] *Istituto di Chimica, Facoltà di Ingegneria, Università, P.le J.F. Kennedy, I-16129, Genova, Italy*
[b] *Departamento de Química Inorgánica, Universidad Complutense, Ciudad Universitaria, E-28040-Madrid, Spain*
[c] *Dipartimento di Ingegneria Idraulica e Ambientale, Università, via Ferrata 1, I-27100 Pavia, Italy*

Received 28th May 1998, Accepted 23rd July 1998

Mn–Ti mixed oxides with composition $Ti_{1-x}Mn_xO_y$ ($x=0$, 0.1, 0.2, 0.5, 0.8, 0.9 and 1) have been prepared. A Mn–TiO_2 monolayer type sample has also been prepared by impregnation, for comparison. Manganese is found to speed up the anatase-to-rutile phase transition, more clearly in the impregnated sample, while titanium tends to slightly hinder the thermodynamically reversible hausmannite-to-bixbyite phase transition upon cooling. The catalytic activity of all samples in propene oxidation decreases by increasing the Ti content. Conversely, the catalytic activity in propane oxidation shows a maximum at intermediate composition.

1 Introduction

Manganese based mixed oxides, such as perovskite-type manganites,[1] Mn-containing β-aluminas,[2] Mn-containing spinels,[3] Mn oxides supported on alumina as powders[4] and on cordierite monoliths[5] and the pure oxides MnO_2,[6–8] Mn_2O_3[9,10] and Mn_3O_4[11] have been proposed as cheap, environmentally friendly and active catalysts for volatile organic compound (VOC) and methane total oxidation processes. They are, however, less active than the more expensive and environmentally demanding catalysts based on noble metals.[5] To increase the activity of oxidation catalysts, supporting the active phase on oxide carriers or mixing it with other oxides is sometimes useful. In particular, TiO_2-anatase is reported to activate V_2O_5 catalysts for several oxidation reactions[12,13] and vanadia–titania based catalysts are used industrially for alkyl aromatic oxidations[14,15] as well as for reducing NO_X with ammonia in the selective catalytic reduction (SCR) process.[16,17] Titania was also reported to activate molybdena and tungsta based catalysts for oxidation[18] and MoS_2 and WS_2 sulfide catalysts for hydro-treating.[19] The nature of such activating effects is still under debate, being either due to the ability of anatase to disperse appropriately the active phases or to optimise their acid–base properties,[20] or due to electronic effects.[21,22]

Supporting or mixing Mn oxides with titania seemed to be a reasonable option to try to improve Mn oxides for oxidation catalysis and to further study the effect of oxide supports with respect to supported oxide catalysis. Mn–Al oxides have been deeply investigated as SCR catalysts.[23,24] Mn–Ti oxides are industrially produced as inorganic pigments[25] and are reported to behave as fairly active and selective catalysts in the oxidation of NH_3 to N_2.[26] In the present paper we will summarise our results on the preparation, characterisation and testing of Mn–Ti complex oxides.

2 Experimental

The preparation of the mixed oxide samples, $Ti_xMn_{1-x}O_y$ ($x=0$, 0.1, 0.2, 0.5, 0.8, 0.9, 1), was carried out by mixing carefully $Mn(CH_3COO)_3{\cdot}2H_2O$ (Acros, 98%) and $Ti[OCH(CH_3)_2]_4$ (Aldrich, 97%) hydrolysing with water, then drying the gel at 393 K for several hours. The subscript x in the notation corresponds to the atomic fraction of Ti in the whole metal content. Another sample was synthesised by a conventional impregnation method, adding an aqueous solution with the required amount of manganese acetate to an aqueous suspension of TiO_2 (Degussa). Then, it was stirred at 373 K until total removal of water, and treated thermally as above.

Nitrates and residual organic compounds were decomposed, in air, in an electronically controlled furnace at 723 K for 4 h. The heating and cooling rate before and upon calcination was 40 K min^{-1}.

XRD spectra were recorded on a Philips PW 1710 diffractometer (Cu-Kα radiation, Ni filter; 45 kV, 35 mA) and cell parameters calculated using dedicated least square software. FTIR spectra were recorded using a Nicolet Magna 750 Fourier Transform instrument. For the region 4000–350 cm^{-1} a KBr beam splitter has been used with a DTGS detector. For the FIR region (600–50 cm^{-1}) a 'solid substrate' beam splitter and a DTGS polyethylene detector were used. KBr pressed disks (IR region) or polyethylene pressed disks and samples deposed on Si disks (FIR region) were used.

FT-Raman spectra were recorded using a Bruker RFS100 Instrument, with an Nd-YAG laser (1064 nm), using 30 mW laser power, 2000 scans and 4 cm^{-1} resolution. Diffuse reflectance spectra in the range 2500–200 nm were obtained with a Jasco V-570 spectrophotometer at room temperature using a polymer as reference. BET surface areas were measured with a conventional volumetric instrument by nitrogen adsorption

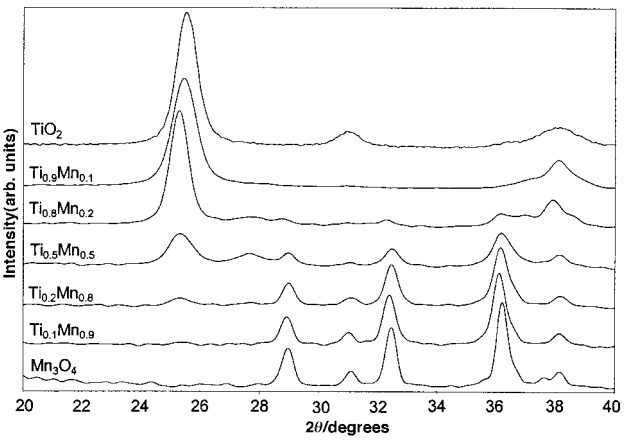

Fig. 1 XRD patterns of the powders after calcination at 773 K.

at liquid nitrogen temperature. DTA–TG experiments were performed in air, with a Setaram TGA 92-12 apparatus, from room temperature to 1273 K, with heating and cooling rates of 10 K min^{-1}.

Catalytic tests were carried out at atmospheric pressure in a continuous flow tubular glass reactor. Variable amounts of catalysts calculated to have the same exposed total surface area (1.83 m^2) were loaded in the form of fine powder (60–70 mesh) mechanically mixed with a predetermined amount of inert, low surface area, material (quartz) to avoid preferential gas flow paths and hot spots in the catalytic bed.

The total gas flow was 330 ml min^{-1} and the feed composition was *ca.* 1.5% of hydrocarbon in oxygen-containing helium. The hydrocarbon/oxygen molar ratio in the feed was 1 : 6. The reactants and the reaction products were analysed using two on-line gas chromatographs (HP 5890), working in different analysis conditions in order to give a better resolution of inorganic and organic species.

3 Catalyst characterisation

3.1 Structural characterisation of the mixed oxide catalysts after calcination at 773 K

Fig. 1 shows the XRD powder patterns of the mixed oxide samples after calcination at 773 K. The observed crystal phases with the measured unit cell parameters are summarised in Table 1. The Mn oxide sample is constituted by the random tetragonal spinel phase α-Mn_3O_4 (hausmannite). This phase alone is also found in the sample $Ti_{0.1}Mn_{0.9}$ and is present in the patterns of all samples up to $Ti_{0.8}Mn_{0.2}$ where it is still detected in traces. From $Ti_{0.2}Mn_{0.8}$ the TiO_2-anatase phase is also observed, and is the only phase detectable in the sample $Ti_{0.9}Mn_{0.1}$. Pure titania is constituted by anatase with small amounts of brookite. Traces of rutile are detected for $Ti_{0.5}Mn_{0.5}$ only. The cell volume of the anatase phase appears to increase with dissolution of Mn in the samples $Ti_{0.9}Mn_{0.1}$ and $Ti_{0.8}Mn_{0.2}$. Conversely, the volume of the hausmannite phase appears to decrease in the samples $Ti_{0.2}Mn_{0.8}$ and $Ti_{0.5}Mn_{0.5}$ suggesting dissolution of Ti in Mn_3O_4.

The skeletal IR and FIR spectra clearly show the typical absorptions of the hausmannite spinel phase for the pure Mn oxide [Fig. 2(g)] with main bands at 611, 524, 421, 245, 165 and 124 cm^{-1}, in good agreement with the results reported by Lutz *et al.*[27] The same absorptions are also observed in the spectra of the Ti-containing samples up to $Ti_{0.5}Mn_{0.5}$ [Fig. 2(d)–(f)], although traces of these absorptions can also be found for $Ti_{0.8}Mn_{0.2}$. In parallel, the broad absorptions of TiO_2 (anatase)[28] are clearly found already for $Ti_{0.2}Mn_{0.8}$ [Fig. 2(a)–(c)]. In the case of Ti the complexity in the range 600–400 cm^{-1} is attributed to the presence of some traces of brookite.[21]

Similarly, the Raman spectra show a peak at 655 cm^{-1}, typical of spinels[20,29] and reported explicitly for hausmannite,[20,30] for pure Mn oxide [Fig. 3(a)] and for samples up to $Ti_{0.8}Mn_{0.2}$ [Fig. 3(b)–(e)]. In the Raman spectrum of $Ti_{0.2}Mn_{0.8}$ the main peak of anatase[21] at 142 cm^{-1} starts to be present. For the sample $Ti_{0.9}Mn_{0.1}$ only the peaks of anatase are found at 638, 512, 395, 322, 236 and 142 cm^{-1}, while for pure TiO_2 traces of brookite (450 and 359 cm^{-1}) are detectable within the pattern of anatase.[21] Thus, both vibrational spectroscopic techniques fully confirm the data arising from XRD summarised in Table 1.

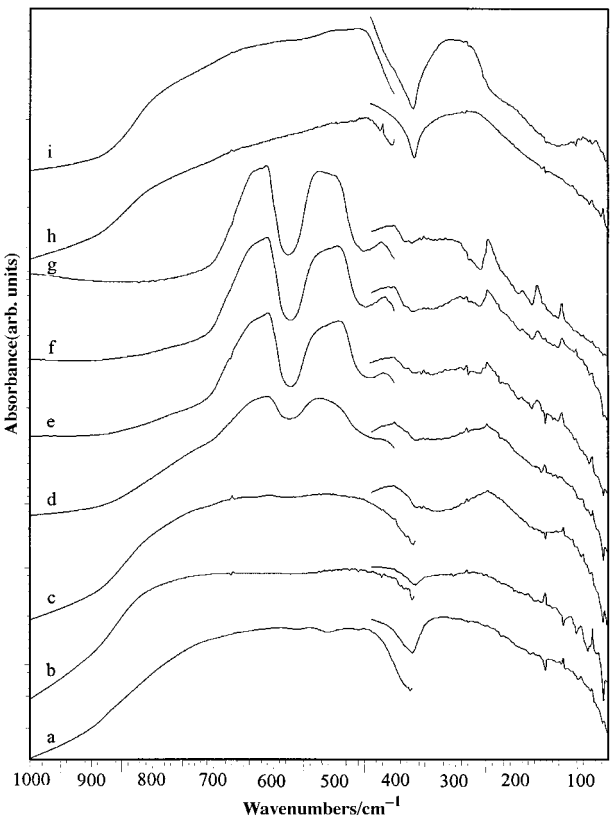

Fig. 2 FTIR/FTFIR skeletal spectra of the powders after calcination at 773 K. (a) TiO_2, (b) $Ti_{0.9}Mn_{0.1}$, (c) $Ti_{0.8}Mn_{0.2}$, (d) $Ti_{0.5}Mn_{0.5}$, (e) $Ti_{0.2}Mn_{0.8}$, (f) $Ti_{0.1}Mn_{0.9}$, (g) Mn_3O_4, (h) 6%Mn-TiO_2 (Degussa), (i) TiO_2 (Degussa).

The specific surface areas, reported in Table 1, show an almost monotonic decrease upon increasing Mn content.

3.2 Study of the thermal stability of mixed oxide catalysts

DTA and XRD studies. The DTA curves for mixed oxide catalysts are shown in Fig. 4. The observed crystal phases with

Table 1 XRD data for $Ti_xMn_{1-x}O_y$ samples at 773 K

Sample	$T_{calc.}$/K	XRD phase(s)	Cell parameters/Å		Volume/Å^3	S_{BET}/m^2 g^{-1}
			a	*c*		
Ti	773	Anatase (Brookite)	3.777(2)	9.460(6)	135.0	94
$Ti_{0.9}Mn_{0.1}$	773	Anatase	3.790(1)	9.446(5)	135.6	83
$Ti_{0.8}Mn_{0.2}$	773	Anatase (Hausmannite)	3.790(1)	9.493(4)	136.4	53
$Ti_{0.5}Mn_{0.5}$	773	Anatase Hausmannite (Rutile)	3.809(6) 5.763(1)	9.434(27) 9.429(5)	136.9 313.0	42
$Ti_{0.2}Mn_{0.8}$	773	Hausmannite (Anatase)	5.761(0)	9.427(3)	313.0	25
$Ti_{0.1}Mn_{0.9}$	773	Hausmannite	5.768(0)	9.446(1)	314.3	18
Mn	773	Hausmannite	5.759(1)	9.443(5)	314.3	11

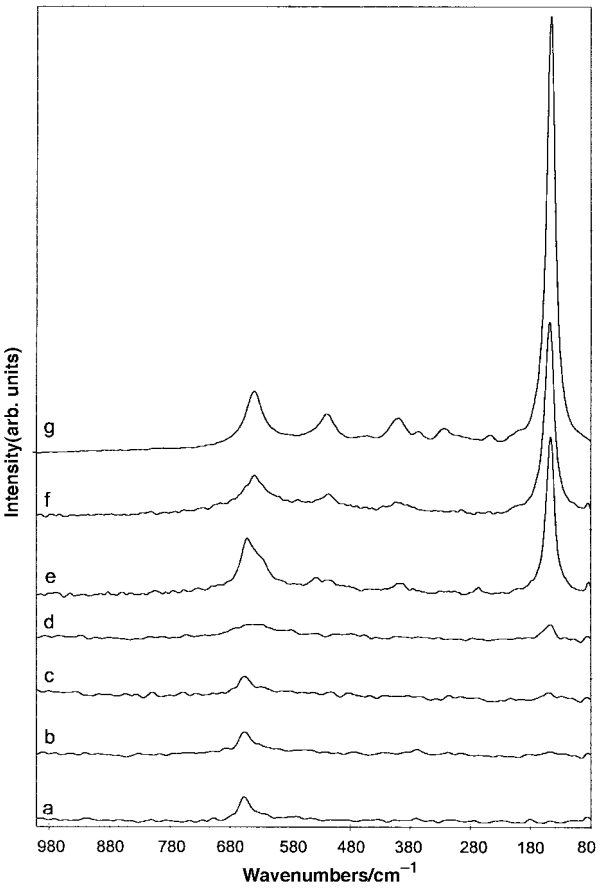

Fig. 3 FT-Raman spectra of the powders after calcination at 773 K. (a) Mn_3O_4, (b) $Mn_{0.9}Ti_{0.1}$, (c) $Mn_{0.8}Ti_{0.2}$, (d) $Mn_{0.5}Ti_{0.5}$, (e) $Mn_{0.2}Ti_{0.8}$, (f) $Mn_{0.1}Ti_{0.9}$, (g) TiO_2 (its intensity value is 10 times greater than for the others).

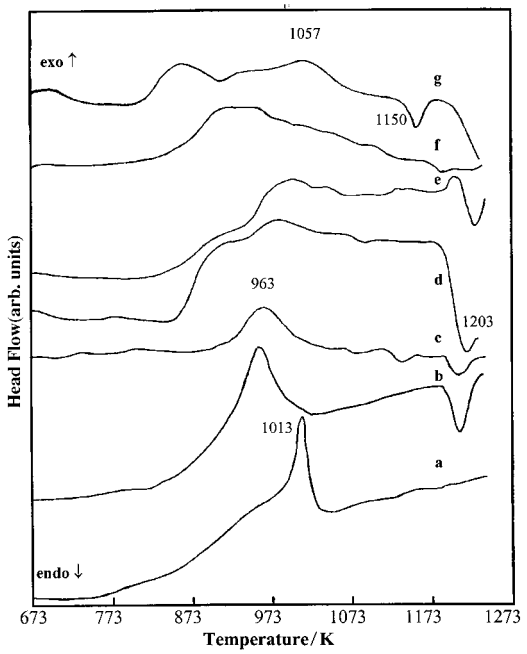

Fig. 4 DTA curves of the powders after calcination at 773 K. (a) TiO_2, (b) $Ti_{0.9}Mn_{0.1}$, (c) $Ti_{0.8}Mn_{0.2}$, (d) $Ti_{0.5}Mn_{0.5}$, (e) $Ti_{0.2}Mn_{0.8}$, (f) $Ti_{0.1}Mn_{0.9}$, (g) Mn_3O_4.

Table 2 XRD data for $Ti_xMn_{1-x}O_y$ samples at 1273 K.

Sample	$T_{calc.}$/K	XRD phase(s)	Cell parameters/Å		Volume/Å^3
			a	*c*	
Ti	1273	Rutile	4.592(0)	2.959(0)	62.4
$Ti_{0.9}Mn_{0.1}$	1273	Rutile	4.589(0)	2.957(0)	62.3
		Pyrophanite	5.139(0)	14.277(5)	326.5
$Ti_{0.8}Mn_{0.2}$	1273	Rutile	4.585(0)	2.956(0)	62.1
		Pyrophanite (Bixbyite)	5.125(1)	14.270(5)	324.6
$Ti_{0.5}Mn_{0.5}$	1273	Pyrophanite	5.136(1)	14.279(3)	326.2
		Rutile (Bixbyite)	4.596(5)	2.943(9)	62.1
$Ti_{0.2}Mn_{0.8}$	1273	Bixbyite	9.425(5)	9.425(5)	837.2
		Pyrophanite (Rutile)	5.118(2)	14.229(24)	322.8
$Ti_{0.1}Mn_{0.9}$	1273	Bixbyite (Rutile)	9.425(1)	9.425(1)	837.2
Mn_3O_4	1273	Hausmannite	5.761(0)	9.450(2)	313.6
Mn_2O_3[a]		Bixbyite	9.430(2)	9.430(2)	838.6

[a]Reference sample.

the measured unit cell parameters after DTA are summarised in Table 2. At the end of the DTA cycle, the Mn oxide is still in the form of Mn_3O_4 (hausmannite), although with a large decrease in the crystal size. By contrast the sample $Ti_{0.1}Mn_{0.9}$ only shows features that must be attributed to α-Mn_2O_3 (bixbyite) with small traces of TiO_2-rutile. A further phase, the mixed oxide $MnTiO_3$ (pyrophanite) present at a trace level in $Ti_{0.2}Mn_{0.8}$, is the predominant phase in $Ti_{0.5}Mn_{0.5}$ and is a minor phase for the sample $Ti_{0.8}Mn_{0.2}$. In the latter sample rutile is the major phase. Unit cell parameters of rutile slightly decrease by increasing Mn content in the mixed phase powder, in agreement with the behaviour for MnO_2–TiO_2 solid solutions.[31] By contrast, bixbyite parameters decrease with respect to a pure reference sample, possibly indicating that some titanium is dissolved in it.

For TiO_2 [Fig. 4(a)] the DTA curve shows a sharp exothermic peak at 1013 K, due to the anatase-to-rutile transition,[32,33] preceded by a broad exothermic feature in the range 873–973 K due to anatase sintering.[34] The anatase-to-rutile phase transition is shifted to *ca.* 963 K in catalysts $Ti_{0.9}Mn_{0.1}$ and $Ti_{0.8}Mn_{0.2}$ [Fig. 4(b) and (c)], and is associated with a very small weight loss detectable in the TG curve (Table 3). A pronounced endothermic peak associated to a weight loss is observed additionally at 1203 K in the DTA curve (Table 3) of catalysts $Ti_{0.9}Mn_{0.1}$ and $Ti_{0.8}Mn_{0.2}$. According to XRD analysis of the samples after the DTA runs up to 1073 and

Table 3 TG data on $Ti_xMn_{1-x}O_y$ samples

Sample	Temperature/K	Weight loss (%)	Weight gain (%)
TiO_2	873–973	—	—
	1013	—	—
$Ti_{0.9}Mn_{0.1}O_y$	963	—	—
	1203	0.65	—
$Ti_{0.8}Mn_{0.2}O_y$	963	—	—
	1203	0.92	—
$Ti_{0.5}Mn_{0.5}O_y$	873–963	0.80	—
	963	—	0.45
	1203	2.61	—
$Ti_{0.2}Mn_{0.8}O_y$	863–1023	—	0.90
	1203	0.45	—
$Ti_{0.1}Mn_{0.9}O_y$	863–1057	—	1.70
	1203	0.30	—
Mn_3O_4	863	—	2.05
	1057	1.40	—
TiO_2 (Degussa)	1083	—	—
6%Mn-TiO_2 (Degussa)	973	—	0.15
	1213	0.35	—

1273 K, these features are due to the reactions first giving rise to Mn_2O_3 from Mn_3O_4 (in fact Mn_3O_4 is metastable with respect to Mn_2O_3 below *ca.* 1253 K)[35] and later producing $MnTiO_3$ (pyrophanite), according to the following stoichiometry:

$$TiO_2 + 1/2\ Mn_2O_3 \rightarrow MnTiO_3 + 1/4\ O_2$$

In the case of $Ti_{0.5}Mn_{0.5}$ [Fig. 4(d)] we again find the features due to the anatase-to-rutile phase transition (963 K) and pyrophanite formation (1203 K). However, we also find a complex situation with weight loss and an exothermic phenomenon, in the range 873–973 K followed by a weight gain during the anatase-to-rutile transition phase. In agreement with the above experiments, during the exothermic anatase sintering, Mn^{3+} oxide species are segregated as Mn_3O_4, with oxygen loss. Later Mn_3O_4 is oxidised to Mn_2O_3 in the range 973–1013 K before reacting with TiO_2 to give pyrophanite. In fact, the only way to explain a weight gain is that part of Mn is oxided.

For the samples with a large content of Mn, no phase transition of anatase is observable while the endothermic peak associated with pyrophanite formation is still observed. Another endothermic peak due to the Mn_2O_3-to-Mn_3O_4 phase transition is found at 1057 K mainly for pure Mn oxide. In fact, according to the thermodynamic phase diagram,[33] Mn_3O_4 is thermodynamically stable above 1253 K. In agreement with this the TG–DTA (Table 3) runs for Mn_3O_4 show first a weight gain at 863 K (metastable-to-stable phase transition) and later a weight loss due to the thermodynamically driven inverse reaction [Fig. 4(g)].

These data show that Mn favours the anatase-to-rutile phase transition. Previous studies showed that other cations such as Cu^{2+}[36] and V^{5+}[32] also favour anatase sintering and the anatase-to-rutile phase transition. Conversely, we reported that Mo^{6+}, Co^{n+},[33] W^{6+},[37] and Si^{4+}[38] tend to hinder both these phenomena. We observed that this behavior is predominantly found when the cations are impregnated at the anatase surface. We interpreted these data by a sintering-induced phase transition mechanism.[33] The data presented here fully agree with previous observations, indicated that Mn^{n+} behaves similarly to V^{5+} and Cu^{2+}. On the other hand, Ti seems to hinder slightly the thermodynamically reversible hausmannite-to-bixbyite phase transition upon cooling.

3.3 Electronic characterisation of mixed oxide catalysts

UV–VIS diffuse reflectance spectra of TiO_2, $Ti_{0.9}Mn_{0.1}$, $Ti_{0.8}Mn_{0.2}$ and $Ti_{0.5}Mn_{0.5}$ are shown in Fig. 5. The electronic spectra of the TiO_2 samples [Fig. 5(a) and (c)] correspond to those reported previously for similar samples[39,40] and other oxide binary systems such as Ti–Sr[41] and Ti–Al.[42] This spectrum is characterized by a strong absorption edge in the range 200–400 nm with two main absorptions at *ca.* 220 and 305 nm which are attributed an O 2p→Ti 3d charge-transfer transition.[43]

In the samples containing Mn, additional absorption appears at higher wavelengths, *i.e.* in the visible region. As a result, the absorption at 305 nm increases in intensity progressively and its position shifts towards higher wavelengths, up to 345 nm for the sample $Ti_{0.8}Mn_{0.2}$ [Fig. 5(e)] before falling to *ca.* 320 nm for $Ti_{0.5}Mn_{0.5}$ [Fig. 5(f)]. Meanwhile, the absorption at 220 nm is shifted to 255 nm for the same samples. Above 400 nm a broad tail appears which becomes more predominant upon increasing the Mn content, with the appearance of higher wavelength components as shoulders at 570 and 760 nm, which is more evident for the sample $Ti_{0.8}Mn_{0.2}$. These two components become indistinguishable when the Mn content is $\geqslant 0.5$.

UV–VIS spectra of samples with greater Mn content are shown in Fig. 6, together those of the pure manganese oxides,

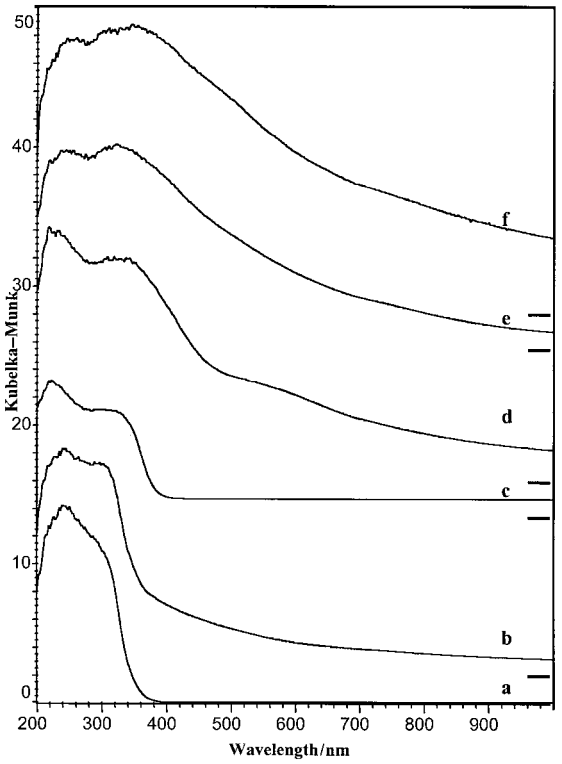

Fig. 5 UV–VIS spectra of the powders after calcination at 773 K. (a) TiO_2 (Degussa), (b) 6%Mn-TiO_2 (Degussa), (c) TiO_2, (d) $Ti_{0.9}Mn_{0.1}$, (e) $Ti_{0.8}Mn_{0.2}$, (f) $Ti_{0.5}Mn_{0.5}$.

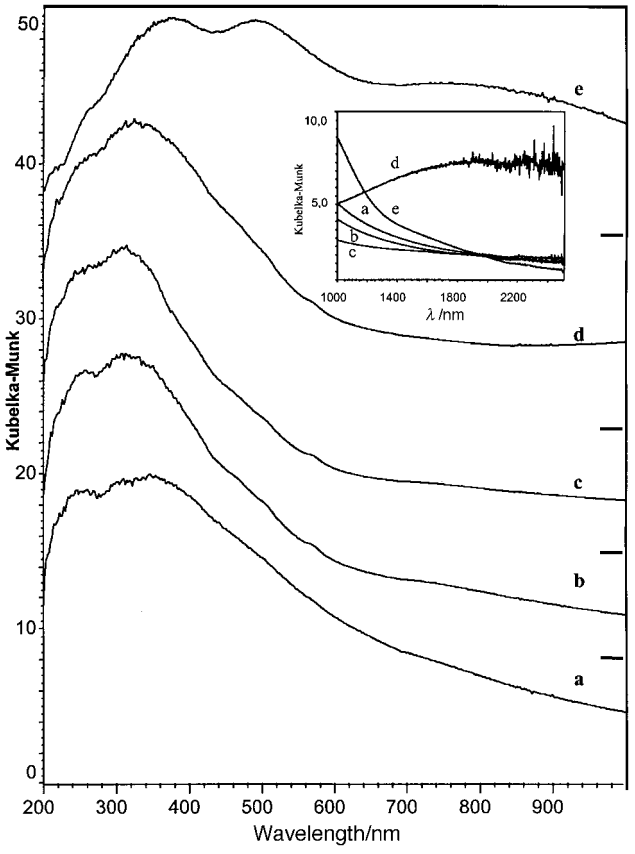

Fig. 6 UV–VIS spectra of the powders after calcination at 773 K. (a) $Ti_{0.5}Mn_{0.5}$, (b) $Ti_{0.2}Mn_{0.8}$, (c) $Ti_{0.1}Mn_{0.9}$, (d) Mn_3O_4, (e) Mn_2O_3 (reference sample).

hausmannite and bixbyite (the latter calcined at 1073 K). In these spectra, the absorption at 255 nm decreases in intensity without shifting till it almost disappears, while the other at 320 nm becomes the predominant component in the range 320–305 nm in the spectrum of Mn_3O_4 [Fig. 6(d)]. As for the components in the region above 400 nm, at least three clear shoulders can be observed at 460, 565 and 740 nm for the Mn–Ti mixed oxides, the last decreasing in intensity with the Mn content. This component disappears in the Mn_3O_4 electronic spectrum, which however also shows a very broad absorption in the NIR region (see insert in Fig. 6). The α-Mn_2O_3 spectrum is formed by three bands at *ca.* 370, 485 and 755 nm.

In the α-Mn_2O_3 structure, Mn^{3+} ions (d^4) occupy octahedral sites and, if highly symmetric, a single spin-allowed absorption band in the d–d transition region is expected similarly to $[Mn(H_2O)_6]^{3+}$ at 500 nm.[44] However, a distortion of the octahedral coordination sphere can give rise to a different splitting of d levels and so other d–d transitions can occur.[45,46] Thus, the absorptions in the bixbyite spectrum can be assigned, in order of increasing wavelength, to a $O^{2-}\rightarrow Mn^{3+}$ charge-transfer transition, to superimposed $^5B_{1g}\rightarrow{}^5B_{2g}$ and $^5B_{1g}\rightarrow{}^5E_g$ crystal-field d–d transitions, and to a $^5B_{1g}\rightarrow{}^5A_{1g}$ crystal-field d–d transition, respectively.[45,46]

The interpretation of the hausmannite spectrum is complex because it shows random cation distribution in the spinel structure. However, some considerations should be taken into account: for instance, Mn^{2+} (d^5) d–d transitions are expected to be weak in both octahedral and tetrahedral sites, since they are, in principle, both spin and orbitally forbidden.[47] According to previous studies[48–51] the absorption band at 255 nm in the spectrum of Mn_3O_4 is associated with a $O^{2-}\rightarrow Mn^{2+}$ charge-transfer transition and that at 320 nm with $O^{2-}\rightarrow Mn^{3+}$ charge-transfer. In the near-IR region, a broad band with a maximum at *ca.* 1750 nm is only found in the hausmannite spectrum. Previous studies[45,46,52] have reported that this band in the spinel structure can be assigned to a $^5E\rightarrow{}^5T_2$ d–d transition of octahedral Mn^{3+} and its major energy with respect to that of the crystal field Δ_o is due to a distortion from octahedral coordination.

In the UV–VIS spectra of Mn–Ti mixed oxide samples, the variation of Mn content explains clearly the decrease of intensity and the shifting of the bands, since these features relate to TiO_2 charge-transfer transitions. The component near 460 nm and the broad absorption centred around 750–760 nm can be related to the absorptions present in the spectrum of α-Mn_2O_3 at *ca.* 485 and 755 nm, suggesting that the majority of manganese is Mn^{3+} in octahedral coordination. However, according to previous studies the apparent shift of the absorption edge in the range near 400 nm in the sample $Ti_{0.9}Mn_{0.1}$ (which only shows the anatase phase with, possibly, dissolved Mn ions, according to XRD) could also be associated to transitions of Mn^{4+} in the TiO_2 phase.[49] The other weak and sharp component near 565 nm can be tentatively assigned to the $^6A_1\rightarrow{}^4T_1$ forbidden d–d transition of Mn^{2+}, either in an octahedral or tetrahedral site.[47]

3.4 Characterisation of the impregnated catalyst after calcination at 773 K

Similar experiments have been performed on a sample prepared by impregnation of a commercial TiO_2 support, from Degussa (anatase + 30% rutile mixture), for comparison. The loaded Mn amount (6% wt./wt.) was calculated to be approximately that needed to cover the overall support surface with a complete 'monolayer'. In the XRD powder pattern of a sample after calcination at 773 K, anatase and rutile phases are present with relative ratios very similar to those of pure support TiO_2, and traces of the bixbyite phase.[53]

Fig. 7 compares DTA curves of the 6%Mn–TiO_2 (Degussa) and TiO_2 (Degussa) samples. The TiO_2 (Degussa) run is characterised by an exothermic peak near 1083 K without appreciable weight loss, as reported in Table 3, due to the anatase-to-rutile phase transition. The addition of Mn produces a notable shift of this peak up to 973 K, indicating that the presence of Mn favours the anatase-to-rutile phase transition, not only in the mixed oxide samples but also if impregnated on the surface. Also, a new endothermic peak appears at 1203 K, which can be associated with pyrophanite formation.

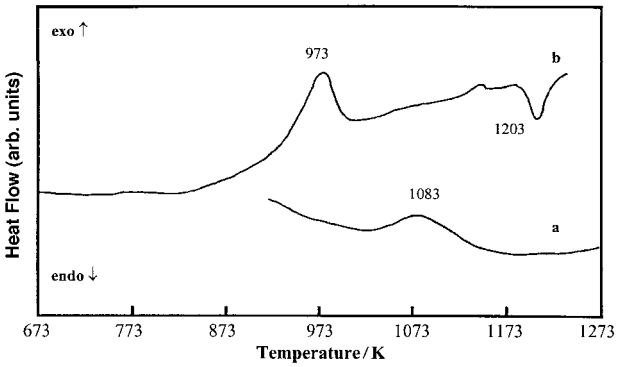

Fig. 7 DTA curves of impregnated samples after calcination at 773 K. (a) TiO_2 (Degussa), (b) 6%Mn-TiO_2 (Degussa).

The FTIR spectra (Fig. 2) of the Degussa support and of the Mn containing sample prepared from it appear to be very similar and both show the strong absorptions of TiO_2. The spectrum in the FIR region does not reveal appreciable traces of Mn oxide phases.

The electronic spectra of the TiO_2 (Degussa) support and of the impregnated catalyst are compared in Fig. 5(a) and (b). When Mn is added, a significant absorption above 400 nm into the visible region is observed in addition to that of the TiO_2 edge. Components can be found near 440 nm, just at the lower energy side of the TiO_2 gap transition, and in the 750 nm region. As discussed above, by comparison with the Mn_2O_3 spectrum, these new features are likely to be due to octahedral Mn^{3+} species. In this case, however, the TiO_2 band gap does not seem to be substantially modified, in contrast with what occurs for mixed oxide samples. This can be associated to the existence, in the case of mixed oxides only, of Mn species dissolved in the TiO_2 bulk.

4 Catalytic tests

All Mn-containing samples are found to be active in the catalytic oxidation of both propane and propene. Propene oxidation is total in all cases giving rise almost exclusively to CO_2 with very small amounts of CO (selectivities always below 5%) and negligible traces of ethylene (<0.1% selectivity). However, the sample activity measured by using the same catalyst surface areas and flow rates, is very sensitive to composition (Fig. 8). Conversion above 97% is achieved on bixbyite at 540 K while on hausmannite such levels of conversion are attained above 600 K. On mixed and supported Mn–Ti oxides 6% or lower conversions are obtained at 700 K. However, comparison of the activities at lower temperatures and conversions (Fig. 8), where the kinetic regime is chemical (as shown by the calculated activation energies of 19 kcal mol^{-1}), shows similar behaviour for the two Mn oxides. This apparently contradicts a previous study from our group, where Mn_3O_4 was reported to be significantly more active than α-Mn_2O_3.[10] However, in that case we measured the activity of samples different than those described here, and characterised by very different surface area and pre-treatment temperatures.

The catalytic activities of both Mn–Ti mixed oxides and of

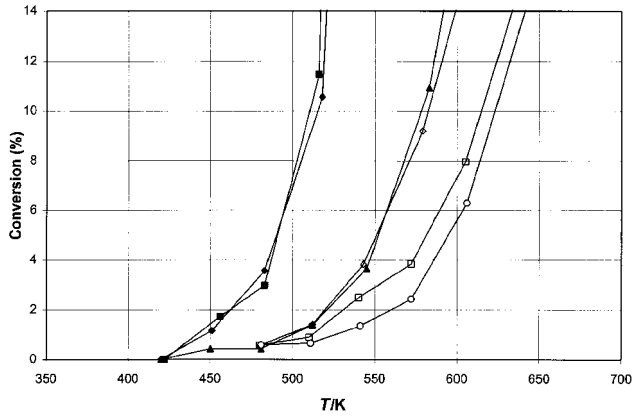

Fig. 8 Propene conversion over manganese and titanium oxides as a function of the reaction temperature. (◆) Mn_3O_4, (■) Mn_2O_3, (▲) $Ti_{0.1}Mn_{0.9}$, (◇) $Ti_{0.2}Mn_{0.8}$, (□) $Ti_{0.5}Mn_{0.5}$, (○) 6%Mn-TiO_2 (Degussa).

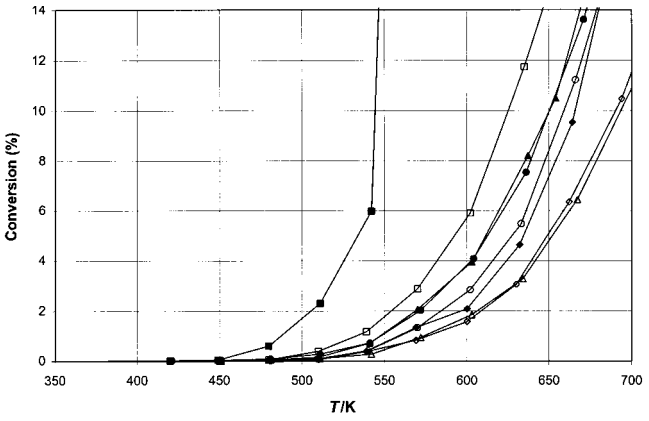

Fig. 9 Propane conversion over manganese and titanium oxides as a function of the reaction temperature. (◆) Mn_3O_4, (■) Mn_2O_3, (▲) $Ti_{0.1}Mn_{0.9}$, (◇) $Ti_{0.2}Mn_{0.8}$, (□) $Ti_{0.5}Mn_{0.5}$, (●) $Ti_{0.8}Mn_{0.2}$, (△) $Ti_{0.9}Mn_{0.1}$, (○) 6%Mn-TiO_2 (Degussa).

the supported catalysts are by far lower than those of the pure Mn oxides. Temperatures of 580 K are needed to obtain 10% propene conversion for the samples $Ti_{0.1}Mn_{0.9}$ and $Ti_{0.2}Mn_{0.8}$, while the same conversion is attained only above 620 K for the sample $Ti_{0.5}Mn_{0.5}$ and by the supported sample.

The conversion of propane is, as expected, lower than that of propene in all cases, under the same conditions (Fig. 9). In this case, however, oxydehydrogenation to propene is predominant at very low conversion and still remains significant up to total propane conversion. CO_2 is the predominant product when propane conversion becomes significant while CO is also formed later. Traces of ethylene are also observed. The behaviour of the supported catalyst 6% Mn-TiO_2 (Degussa) is shown in Fig. 10, and can be regarded as representative of all Mn-containing samples. A similar behaviour has been described previously for bulk Mn oxides.[10,11] By comparing again the activities at lower conversions (Fig. 9), we find that the catalytic activity of α-Mn_2O_3 (bixbyite) is in this case far higher than that of Mn_3O_4 (hausmannite). Mn_3O_4 is, however, more selective towards propene at similar conversion, giving yields of propene of the order of 5% under these conditions. Again CO is produced in very small amounts (selectivity $<5\%$), CO_2 being predominant.

The mixed oxide samples show catalytic activity higher than Mn_3O_4 although lower than for Mn_2O_3. The catalytic activity of the supported catalyst does not differ significantly from those of mixed oxide catalysts, and also the sample $Ti_{0.9}Mn_{0.1}$ shows significant oxidation activity. The trends for propane conversion activity and propene selectivities are quite difficult to rationalise for Mn–Ti mixed oxides, with a maximum in activity for the

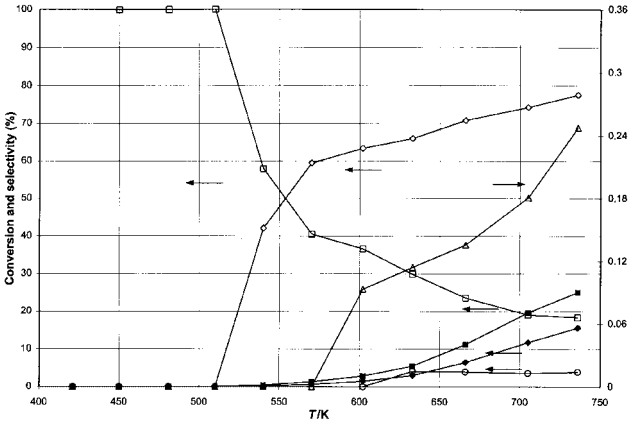

Fig. 10 Product reaction upon propane oxidation as a function of the reaction temperature over 6%Mn-TiO_2 (Degussa). (◆) O_2 (conv.), (◇) CO_2 (sel.), (■) C_3H_8 (conv.), (□) C_3H_6 (sel.), (○) CO (sel.), (△) C_2H_4 (sel.).

sample $Ti_{0.5}Mn_{0.5}$ and a maximum in selectivity to propane for $Ti_{0.2}Mn_{0.8}$.

Conclusions

Conclusions from the above data are as follows.

1 The addition of Ti to Mn oxide favours the formation of the thermodynamically stable phase α-Mn_2O_3 (bixbyite) with respect to that of the metastable phase (at room temp.) Mn_3O_4 (hausmannite).

2 Ti apparently enters the bixbyite phase in small amounts.

3 Mn addition, both in the samples of mixed oxides and the supported catalyst, favours the anatase-to-rutile phase transitions. This effect is particularly evident for impregnation, in agreement with the sintering-induced phase-transition effect, previously proposed by some of us.[33]

4 Mn enters the TiO_2 anatase phase in small amounts, in the samples of mixed oxides.

5 The pyrophanite phase $MnTiO_3$ is produced by heating Mn-mixed oxides above 1200 K.

6 The surface areas of mixed Mn–Ti oxides tend to decrease upon increasing the Mn content.

7 Characterisation of a supported Mn-TiO_2 catalyst shows that Mn oxide species are well dispersed, with α-Mn_2O_3 (bixbyite) particles only detectable in traces.

8 UV–VIS spectra suggest that surface Mn oxide species on TiO_2 are mainly constituted of octahedrally coordinated Mn^{3+} species.

9 Mixed and supported Mn–Ti oxides are active and selective catalysts for the total oxidation of propene to CO_2. By contrast, they give rise to substantial partial oxidation products like propene and CO upon oxidation of propane after partial conversion.

10 Mixing Mn oxides with, or supporting on, TiO_2 strongly deactivates them for propene oxidation. As for propane oxidation, mixed Mn–Ti oxides are by far less active than α-Mn_2O_3 (bixbyite) but can be more active than Mn_3O_4 (hausmannite).

11 The activation effect of TiO_2 on vanadia, molybdena and tungsta oxidation catalysts does not occur on Mn oxides. This can be interpreted assuming that this effect is not due to the ability of TiO_2 anatase to disperse the active phase (occurring in both cases), but rather to different electronic effects that distinguish oxides of d^0 cations (*e.g.* vanadia, molybdena and tungsta) from the oxides of d-electron containing cations.

Acknowledgements

Part of this work has been supported by NATO (CRG-960316). J. M. G. A. acknowledges MEC for a FPI grant.

References

1 P. E. Marti, M. Maciejewski and A. Baiker, *Appl. Catal.*, *B: Environ*., 1994, **4**, 225.
2 G. Groppi, M. Bellotto, C. Cristiani and P. Forzatti, *Appl. Catal.*, *A: General*, 1993, **104**, 101.
3 H. G. Lintz and K. Wittstock, *Catal. Today*, 1996, **29**, 457.
4 U. S. Ozkan, R. F. Kueller and E. Moctezuma, *Ind. Eng. Chem. Res*., 1990, **29**, 1136.
5 J. Carnö, M. Ferrandon, E. Björnbom and S. Järäs, *Appl. Catal.*, *A: General*, 1997, **155**, 265.
6 G. K. Boreskov, B. I. Popov, V. N. Bibin and E. S. Kozishnikova, *Kinet. Katal.*, 1968, **9**, 796.
7 J. E. Germain and R. Perez, *Bull. Soc. Chim. Fr.*, 1972, 4683.
8 C. Lahousse, A. Bernier, A. Gaigneaux, P. Ruiz, P. Grange and B. Delmon, in *3rd World Congress on Oxidation Catalysis*, ed. R. K. Grasselli, S. T. Oyama, A. M. Gaffney and J. E. Lyons, Elsevier, Amsterdam, 1997, p. 777.
9 J. E. Germain and R. Perez, *Bull. Soc. Chim. Fr.*, 1972, 541; 2042.
10 M. Baldi, V. Sanchez-Escribano, J. M. Gallardo-Amores, F. Milella and G. Busca, *Appl. Catal.*, *B: Environ*., 1998, **17**, L175.
11 M. Baldi, E. Finocchio, F. Milella and G. Busca, *Appl. Catal.*, *B: Environ*., 1998, **16**, 43.
12 P. J. Gellings in *Catalysis*, The Royal Society of Chemistry, London, 1985, vol. 7, p. 105.
13 *Vanadia catalysts for selective oxidation of hydrocarbons and their derivatives*, ed. B. Grzybowska-Swierkosz, F. Trifiró and J. C. Vedrine, Special issue of *Appl. Catal.*, *A: General*, 1997, **157**, 1–426.
14 V. Nikolov, D. Klissurski and A. Anastasov, *Catal. Rev. Sci. Eng*., 1991, **33**, 319.
15 C. R. Dias, M. F. Farinha-Portela and G. C. Bond, *Catal. Rev. Sci. Eng*., 1997, **39**, 169.
16 P. Forzatti and L. Lietti, *Heterog. Chem. Rev*., 1996, **3**, 33.
17 G. Busca, L. Lietti, G. Ramis and F. Berti, *Appl. Catal.*, *B: Environ*., in press.
18 D. Vanhove, S. R. Op, A. Fernandez and M. Blanchard, *J. Catal*., 1979, **57**, 253.
19 J. Ramirez, S. Fuentes, G. Diaz, M. Vrinat, M. Breysse and M. Lacroix, *Appl. Catal*., 1989, **52**, 211.
20 I. E. Wachs, *Catal. Today*,1996, **27**, 437.
21 L. J. Alemany, L. Lietti, N. Ferlazzo, P. Forzatti, G. Busca, E. Giamello and F. Bregani, *J. Catal*., 1995, **155**, 117.
22 M. C. Paganini, L. Dell'Acqua, E. Giamello, L. Lietti, P. Forzatti and G. Busca, *J. Catal*., 1997, **166**, 195.
23 W. S. Kiljlstra, E. K. Poels, A. Bliek, B. M. Weckhuysen and R. A. Schoonheydt, *J. Phys. Chem. B*, 1997, **101**, 309.
24 L. Singoredjo, R. Korver, F. Kapteijn and J. A. Moulijn, *Appl. Catal.*, *B: Environ.*, 1992, **1**, 297.
25 J. R. Hackman, in *Pigment Handbook*, ed. P. A. Lewis, 1998, vol. 1, p. 383.
26 A. Wollner, F. Lange, H. Schmelz and H. Knozinger, *Appl. Catal.*, *A: General*, 1993, **94**, 181.
27 H. D. Lutz, B. Muller and H. J. Steiner, *J. Solid State Chem.*, 1991, **90**, 54.
28 G. Busca, G. Ramis, J. M. Gallardo Amores, V. Sanchez Escribano and P. Piaggio, *J. Chem. Soc.*, *Faraday Trans.*, 1994, **90**, 3181.
29 M. I. Baraton, G. Busca, V. Lorenzelli and R. J. Willey, *J. Mater. Sci. Lett*., 1994, **13**, 275.
30 M. C. Bernard, A. Hugot-Le Goff, B. Vu Thi and S. Cordoba de Torresi, *J. Electrochem. Soc*., 1993, **140**, 3065.
31 M. Valigi and A. Cinimo, *J. Solid State Chem*., 1975, **12**, 135.
32 G. Oliveri, G. Ramis, G. Busca and V. Sanchez Escribano, *J. Mater. Chem*., 1993, **3**, 1239.
33 J. M. Gallardo Amores, V. Sanchez Escribano and G. Busca, *J. Mater. Chem*., 1995, **5**, 1245.
34 J. L. Hébrard and P. Nortier, *J. Am. Cem. Soc.*, 1990, **73**, 79.
35 R. Mtselaar, R. E. J. Van Tol and P. Piercy, *J. Solid State Chem*., 1981, **38**, 335; S. E. Dorris and T. O. Mason, *J. Am. Ceram. Soc*., 1988, **71**, 379.
36 J. M. Gallardo Amores, V. Sanchez Escribano, G. Busca and V. Lorenzelli, *J. Mater. Chem.*, 1994, **4**, 965.
37 G. Ramis, G. Busca, C. Cristiani, L. Lietti, P. Forzatti and F. Bregani, *Langmuir*, 1992, **8**, 1744.
38 Li Yi, G. Ramis, G. Busca and V. Lorenzelli, *J. Mater. Chem.*, 1994, **4**, 1755.
39 H. Bevan, S. V. Dawes and R. A. Ford, *Spectrochim. Acta*, 1958, **13**, 43.
40 T. R. N. Kutty, R. Vivekanan and P. Murugaraf, *Mater Chem. Phys*., 1988, **19**, 533.
41 T. R. N. Kutty and M. Avulaithai, in *Properties and Applications of Perovskite-type Oxides*, ed. L. G. Tejuca and J. L. G. Fierro, Marcel Dekker, New York, 1993, p. 307; L. G. J. DeHaart, A. J. DeVries and G. Blasse, *J. Solid State Chem*., 1985, **59**, 291; J. M. Gallardo-Amores, V. S. Escribano, M. Daturi and G. Busca, *J. Mater. Chem*., 1996, **6**, 879.
42 G. Pacheco-Malagón, A. García-Bórquez, D. Coster, A. Sklyarov, S. Petit and J. J. Fripiat, *J. Mater. Res.*, 1995, **10**, 1264; A. Gutierrez, M. Trombetta, G. Busca and J. Ramirez, *Microporous Mater.*, 1997, **12**, 79.
43 J. K. Burdett, T. Hughbanks, G. J. Miller, J. W. Richardson and J. V. Smith, *J. Am. Cem. Soc*., 1987, **109**, 3639.
44 F. A. Cotton and G. Wilkinson, *Inorganic Chemistry*, John Wiley and Sons, New York, 3rd edn., 1980, p. 765.
45 V. S. Stubican and C. Greskovich, *Geochim. Cosmochim. Acta*, 1975, **39**, 875.
46 F. Lavalille, D. Gourier, A. M. Lejus and D. Vivien, *J. Solid State Chem*., 1983, **49**, 180.
47 *Chemistry of the Elements*, ed. N. N. Greenwood and A. Earnshaw, Pergamon, Oxford, 5th edn., 1995, p. 1231.
48 N. Islam, *Appl. Spectrosc*., 1973, **27**, 285.
49 D. Cordischi, M. Valigli, D. Gazzoli and V. Indovina, *J. Solid State Chem*., 1975, **15**, 82.
50 J. R. Akrige and J. H. Kennedy, *J. Solid State Chem*., 1979, **29**, 63.
51 M. Lenglet, M. Bizi and C. K. Jorgensen, *J. Solid State Chem*., 1990, **86**, 82.
52 R. G. Burns, *Am. Mineral*., 1970, **55**, 1608.
53 J. M. Gallardo Amores, V. Sanchez Escribano, G. Ramis and G. Busca, *Appl. Catal.*, *B: Environ.*, 1997, **13**, 45.

Paper 8/03994A